Use of cw-CRDS for studying the atmospheric oxidation of acetic acid in a simulation chamber

ARTICLE *in* APPLIED PHYSICS B · NOVEMBER 2006

Impact Factor: 1.86 · DOI: 10.1007/s00340-006-2319-6

6 AUTHORS, INCLUDING:

Sabine Crunaire
Ecole des Mines de Douai
22 PUBLICATIONS **96** CITATIONS
SEE PROFILE

Christa Fittschen
CNRS - Université Lille 1
113 PUBLICATIONS **1,356** CITATIONS
SEE PROFILE

Alexandre Tomas
Ecole des Mines de Douai
41 PUBLICATIONS **241** CITATIONS
SEE PROFILE

Patrice Coddeville
Ecole des Mines de Douai
55 PUBLICATIONS **403** CITATIONS
SEE PROFILE

Appl. Phys. B 85, 467–476 (2006)
DOI: 10.1007/s00340-006-2319-6

Applied Physics B
Lasers and Optics

S. CRUNAIRE[1,2]
J. TARMOUL[1,2]
C. FITTSCHEN[1]
A. TOMAS[2,✉]
B. LEMOINE[3]
P. CODDEVILLE[2]

Use of cw-CRDS for studying the atmospheric oxidation of acetic acid in a simulation chamber

[1] Laboratoire de Physico-Chimie des Processus de Combustion et de l'Atmosphère – CNRS UMR 8522, Université des Sciences et Technologies de Lille, Lille I, Bât. C11, 59655 Villeneuve d'Ascq Cedex, France
[2] Département Chimie et Environnement, Ecole des Mines de Douai, 941 Rue Charles Bourseul, B.P. 10838, 59508 Douai Cedex, France
[3] Laboratoire de Physique des Lasers, Atomes et Molécules – CNRS UMR 8523, Université des Sciences et Technologies de Lille, Lille I, Bât P5, 59655 Villeneuve d'Ascq Cedex, France

Received: 30 March 2006/Revised version: 9 May 2006
Published online: 24 June 2006 •

ABSTRACT The coupling between cavity ring-down spectroscopy (CRDS) and an environmental chamber in the investigation of photo-induced reaction mechanisms is demonstrated for the first time.

The development of the CRDS device and the corresponding analytical performances are presented. The first application is devoted to the investigation of the branching ratio of the •OH radical reaction of $CH_3C(O)OH$ and $CH_3C(O)OD$ under tropospheric conditions. An environmental chamber coupled to two complementary detection systems is used:

– gas chromatography with FTIR spectroscopy for quantitative detection of acetic acid;
– CRDS for quantitative detection of CO_2.

Investigation of the reaction kinetics of $^{\bullet}OH + CH_3C(O)OH$ gives a rate constant of $(6.5 \pm 0.5) \times 10^{-13}$ cm^3 molecule^{-1} s^{-1} (296 K) and shows good agreement with literature data. The product study indicates that the H-abstraction channel from the acid group is the dominant pathway with a branching ratio of $(78 \pm 13)\%$, whereas the corresponding D-abstraction channel in the $^{\bullet}OH + CH_3C(O)OD$ reaction represents only $(36 \pm 7)\%$. This result could be attributed to a strong kinetic isotope effect. Glyoxylic acid has also been detected for the first time as by-product.

These results illustrate the high interest of the CRDS technique in the investigation of atmospheric relevant problems.

PACS 82.33.Tb; 82.20.-w; 82.20.Tr; 07.60.-j; 07.88.+y; 42.55.Px; 42.60.Da; 42.62.Fi

1 Introduction

Oxygenated volatile organic compounds are trace components in the atmosphere, with ppt- to ppb-level concentrations encountered in various areas [1–4]. Nevertheless, their impact on the air quality and on the oxidative capacity of the atmosphere through the HO_x budget is considered to be significant, as oxygenated compounds are fairly reactive (with •OH radicals or via sunlight photolysis for carbonyls) [5] and some of them are potentially toxic [6].

✉ Fax: +33327712914, E-mail: tomas@ensm-douai.fr

Recent evidence suggests that carboxylic acids are one of the dominant classes of organic compounds found in the atmosphere, since they are present in a variety of phases (rainwater, vapor phase, aerosols, haze and dew) and they contribute to approximately a quarter of the non-methane hydrocarbon (NMHC) atmospheric mixture ([7, 8] and references therein).

Among these compounds, low molecular weight carboxylic acids like acetic acid have been recognized as potentially important especially in urban polluted atmospheres where concentrations can exceed 20 μg m^{-3} [9] and may be harmful to environment due to the acidification of the natural compartments [10, 11] and to their toxicity towards people health [12].

In the conditions of the lower troposphere, biomass burning and acetylperoxy radical reactions are recognized to be the two main sources of acetic acid [13, 14]. In particular, the reaction of $CH_3C(O)O_2^{\bullet}$ with $HO_2^{\bullet}$ is known to lead to about 20% $CH_3C(O)OH$ [15]. Acetic acid in the atmosphere can also be produced by the reaction of ozone with various olefins like propene, butene [16] or isoprene [17]. A total photochemical source strength of 120×10^{12} g year^{-1} is reported [18]. The contribution of direct emissions from anthropogenic (biomass combustion, motor exhaust) and biogenic (bacteria metabolisms, emission from soil and vegetation) sources is evaluated to 48×10^{12} g year^{-1} [7].

Apart from its atmospheric sink through incorporation in water droplets, the main loss of $CH_3C(O)OH$ is its reaction with •OH radicals:

$$^{\bullet}OH + CH_3C(O)OH \rightarrow \text{products}\,. \qquad (1)$$

The corresponding reaction rate is now fairly well known with a recommended value of $k_1 = 8 \times 10^{-13}$ cm^3 molecule^{-1} s^{-1} at $T = 298$ K [19], the most recent study of Butkovskaya et al. (2004) [20] showing a consistent overall rate constant of 6.6×10^{-13} cm^3 molecule^{-1} s^{-1} at 298 K. Assuming a typical tropospheric •OH concentration of 2×10^6 molecule cm^{-3} [21], an atmospheric residence time ($\tau = 1/k_1 \times [^{\bullet}OH]$) of more than a week can be calculated. The photooxidation chain of acetic acid is expected to contribute to the production of photooxidants, thus influencing the atmospheric HO_x budget [16]. However, models usually do not

take these effects into account because too little is known about the gaseous fate of $CH_3C(O)OH$ in the atmosphere. Therefore, to assess its tropospheric impact, the determination of the product distribution is needed.

Two H-abstraction channels are expected to occur in the $^{\bullet}OH$-initiated oxidation of acetic acid:

$$^{\bullet}OH + CH_3C(O)OH \rightarrow CH_3C(O)O^{\bullet} + H_2O \rightarrow CH_3^{\bullet} + CO_2 + H_2O \quad (1a)$$

$$\rightarrow {}^{\bullet}CH_2C(O)OH + H_2O\,. \quad (1b)$$

The rate coefficients determined by Singleton et al. (1989) [22] for the reactions of $^{\bullet}OH$ radicals with $CH_3C(O)OH$, $CD_3C(O)OH$ and $CD_3C(O)OD$ show that the major reaction channel involves H- (or D-) atom abstraction from the carboxylic group at room temperature. This was confirmed by the branching fraction k_{1a}/k_1 of (64 ± 17) % determined by Butkovskaya et al. (2004) [20] over the temperature range 249–300 K and at a total pressure of 200 Torr using a high-pressure flow reactor. More recently, De Smedt et al. (2005) [23] established a branching fraction of (64 ± 14) % at 290 K and 2 Torr for the channel (1a) using a multistage flow reactor.

In order to get insight in the $^{\bullet}OH + CH_3C(O)OH$ mechanism and to extend the pressure range, we report here a determination of the branching ratio of acetic acid oxidation by hydroxyl radicals at atmospheric conditions (296 ± 2 K and 760 Torr) in an environmental simulation chamber. For a still better understanding of the mechanism, complementary experiments using $CH_3C(O)OD$ were carried out, thus allowing a comparison of the branching ratio obtained in the oxidation of the deuterated acetic acid to that obtained for the non-deuterated in the same experimental conditions.

The gas chromatography (GC) technique coupled to a Fourier transform infrared spectrometer (FTIR) was used to record acetic acid concentrations and continuous-wave cavity ring down spectroscopy (cw-CRDS) to measure CO_2 formation. The cw-CRDS analytical system was developed for the purpose to be coupled to the simulation chamber. This coupling is the first reported to our knowledge and will be described in details in the next sections.

The CRDS technique [24] is now well established as a highly sensitive way to measure weak absorption spectra. Since its discovery in 1997 [25, 26], cw-CRDS and related methods [27, 28] have been used to measure the concentration of several compounds of atmospheric relevance, as reviewed recently by Atkinson [29] and Brown [30]. The measurement of species including CH_4, NO_2, NO_3, NH_3, HCHO and CO_2 [31–36] has been demonstrated to be feasible. The detection of CO_2 at the ppm-level has also been carried out in the near-infrared range by the group of Miller [37]. The spectroscopic parameters (intensities, frequencies, etc.) of this molecule are also well known in the near infrared range [38, 39].

2 Experimental section

2.1 *Experiments in the simulation chamber*

Experiments were carried out in a 300 L Teflon environmental chamber enclosed in a temperature-controlled housing and surrounded by two sets of black lamps (6 tubes Philips TMX 204 LS with emission centred on 254 nm and 6 tubes Philips TMX 200 LS with emission centred on 365 nm), distributed on both chamber sides.

Acetic acid $CH_3C(O)OH$ (Acros Organics > 99%) or partly deutered acetic acid $CH_3C(O)OD$ (Acros Organics > 98% of D-atom) was introduced in the environmental chamber using a gently heated ($T \sim 330$ K) vacuum line (100 mbar) and a slight flow of purified air produced by a zero air generator (Claind 2301 HG). Initial concentrations of acetic and partly deutered acetic acid fall in the range $(3.2 - 6.9) \times 10^{15}$ molecule cm^{-3}.

Hydroxyl radicals were produced by the photolysis of methyl nitrite (CH_3ONO) around 365 nm. CH_3ONO was synthesized using the method described by Taylor et al. [40] and kept at 255 K until use. Generally, 2 to 3 aliquots of tens of mL of gaseous CH_3ONO (resulting in CH_3ONO concentrations of about 4×10^{15} molecule cm^{-3} in the reactor) were introduced in the chamber in the course of the experiment in order to increase the $^{\bullet}OH$-oxidation rate of acetic acid.

Before the reaction was initiated by turning on the lights, the primary gas components were allowed to mix within the chamber for approximately one hour and several samplings of the reaction mixture were analysed in order to determine the accurate initial reactant concentration as well as to test for possible dark reactions. Negligible loss (< 2%) of acetic acid or of its d_1-isotope has been observed. Then the bag was irradiated for two to four hours and sampling was performed at short and steady time intervals (between 15 and 30 min). After each run, the mixture was evacuated; then the bag was cleaned by flushing it with purified air for three times.

2.2 *Instrumentation*

Two different techniques have been used to analyse the reaction mixture. The $CH_3C(O)OH$ and $CH_3C(O)OD$ concentrations were determined using a GC-FTIR analytical device, whereas those of the reaction product CO_2 were measured by the cw-CRDS technique recently developed in our laboratory.

GC-FTIR. The GC-FTIR analytical device is equipped with a thermal desorption system (TCT Chrompack) allowing a 40 mL gas aliquot sampled from the photoreactor (via a sample loop) to be cryotrapped and further injected in the gas chromatographic instrument. A 50-m CP Sil 5 CB capillary column was used for the chromatographic separation combined with the following temperature program: temperature held at 50 °C during 2 min, then increased from 50 °C to 200 °C at a rate of 15 °C min^{-1} and held at 200 °C for 2 min.

Data acquisition was performed using the Omnic software (Nicolet). The Gram–Schmitt chromatogram (from the total spectral response) was built from spectra registered at steady time intervals (every 1.2 s from the average of 10 interferograms). The spectral domain of integration covers the 650 to 4000 cm^{-1} range with a resolution of 16 cm^{-1}. Functional group chromatograms were extracted from the Gram–Schmitt chromatogram in the 1600–1900 cm^{-1} spectral region (C = O band) to carry out the quantitative analysis of acetic acid.

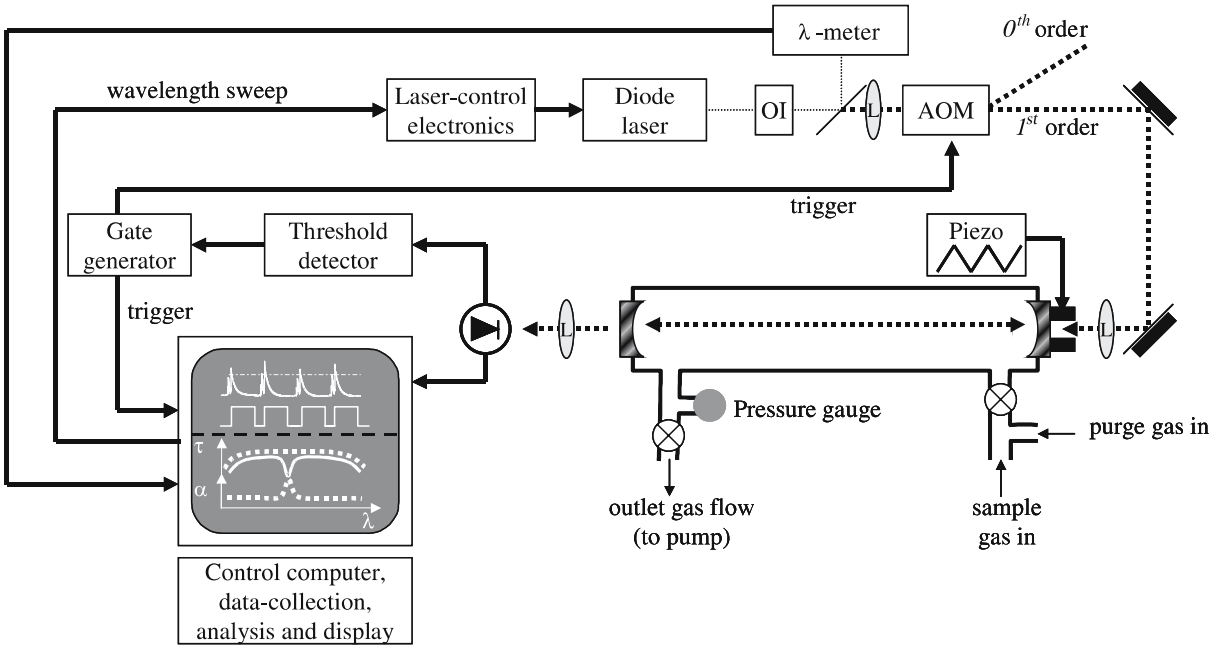

FIGURE 1 Schematic diagram of the cw-CRDS system showing the laser beam (*dashed line*: in fiber optic; *squared line*: open path) from the DFB diode laser through the high finesse cavity (absorption cell) to give the ring-down signal. Just behind the diode laser, a small fraction of the beam intensity is splitted off to calibrate and record the wavelength scale using a lambdameter. OI: optical isolator; L: lens; AOM: acousto–optic modulator

cw-CRDS. Our cw-CRDS experimental apparatus is very similar to that described by Romanini et al. [26] and is illustrated in Fig. 1. It works with a cw-distributed feedback (DFB) diode laser as a light source for excitation of a high finesse optical cavity. The diode laser (NEL – NLK 1556STB) operates over the wavelength range 1569–1576 nm and generates 20 mW of laser power at the most. A fiber-coupled optical isolator (OPTIWORK – ISAD5) was placed after the laser output to reduce laser instability due to feedback into the diode laser. The laser beam was split into a zero and first order deflected beam by an acousto–optic modulator (AOM, Gooch and Housego – M040, 40 MHz), with the latter beam delivered to the ring-down cavity by a set of two mirrors. The laser beam was spatially matched to the TEM_{00} mode of the cavity using a 30 cm focal length lens mounted on a three-dimensional translating stage. Light escaping the opposite end of the cavity was collected by a lens (focal = 5 cm) and focused onto a fast-response, near-infrared avalanche photodiode (EG&G – C30662E, 200 MHz).

For the cavity mirrors, we used a pair of dielectric coated mirrors (Layertec – A0404025) with 1 m radius of curvature and optimised for maximum reflectivity at 1570 nm. They were held within adjustable mounts, placed at a distance L of 72 cm apart on an optical breadboard and stabilised by an assembly of three Invar rods. These mirrors sealed a glass cell equipped with three ports for pressure gauge (Baratron), vacuum pumping line and gas inlets. The cavity mirrors have a reflectivity of 99.978%, which provides an effective optical absorption path length of more than 3 km.

Frequency coincidence of the cavity resonance to the laser frequency is achieved by means of a ring-shaped piezoelectric transducer (Physik Instrumente) attached to one of the mirrors. In this way, the cavity length was continuously modulated at 50 Hz to sweep the cavity mode frequencies back and forth over one free spectral range ($\sim$ 215 MHz). Each time the transmitted light exceeds a predefined threshold indicating optimum coincidence of cavity mode and laser frequency, a trigger pulse is provided to rapidly extinguish the first-order deflected beam via the AOM, thus switching off further build-up of light intensity within the cavity. The subsequent ring-down event is captured by the detector, amplified and recorded by means of an analog-to-digital converter card (National Instrument PCI-6111, 12-bit vertical resolution) connected to a PC. The custom written LabVIEW program fitted each individual ring-down signal to single exponential functions, thus providing the decay time τ for each event. The program was also used to calculate the residual standard deviation of a group of decay rates to test the cavity stability and enable calculation of the detection sensitivity. By measuring the decay time τ_0 of the empty cell and the decay time τ of the cell containing the smog chamber sample (at reduced pressure of 40 Torr to reduce the broadening of spectral lines and thus increase the selectivity), the absorbance $\alpha(\lambda)$, and therefore the concentration can be directly determined using the following equation [41]:

$$\alpha(\lambda) = \sigma_{\text{abs}}(\lambda)[\text{abs}] = \frac{1}{c}\left(\frac{1}{\tau(\lambda)} - \frac{1}{\tau_0}\right),$$

with c the speed of light, $\sigma_{\text{abs}}(\lambda)$ the absorption cross-section at wavelength λ and [abs] the concentration of the absorbent of interest.

To record a spectral line, the laser wavelength was scanned slowly across the range of interest by increasing the input voltage of the laser current driver. The laser wavelength was continuously monitored by a wavemeter (Burleigh – WA-1100).

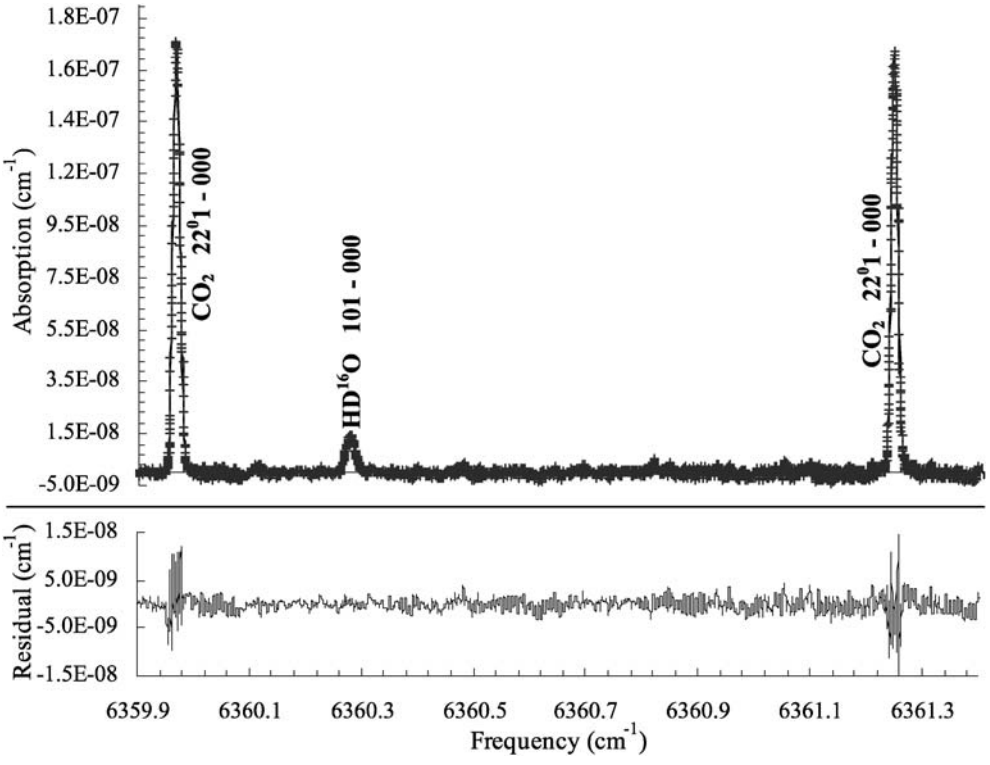

FIGURE 2 Comparison of the cw-CRDS spectrum of a sample of ambient air (*pluses*) at $P = 9.5$ Torr and $T = 296$ K with a simulated spectrum calculated with HITRAN 2004 data using $[CO_2] = 365$ ppmV and a relative humidity of 40% (*solid line*). The residual is displayed on the *lower panel*

2.3 *Determination of the concentrations (* CO_2, CH_3COOH *and* CH_3COOD*) and detection limits*

CO_2. For quantitative determination of the CO_2 concentrations in the photoreactor, the reaction mixture was pumped through the cavity at a flow rate of 70 mL min^{-1} using PTFE tubing.

Figure 2 shows characteristic spectral lines of CO_2 from a sample of ambient air around 6360 cm^{-1} (~ 1572 nm) obtained by cw-CRDS without any average of spectra but with an average of approximately 50 ring down events for each point on the spectrum. On the same figure, we can also see an absorption spectral line of HDO, which can prove the sensibility of the cw-CRDS technique as this species represents less than 0.03% of the water vapor content. From this measurement, the corresponding concentrations can be calculated using the database HITRAN 2004 [39, 42]. Approximately 30 min are needed to scan a spectrum like that presented in Fig. 2. However, for real-time detection, it is sufficient to measure the absorption over a tighter wavelength range (less than 5×10^{-3} nm around the top of the spectral line). In this case, CO_2 concentrations can be determined within a few seconds. It should be pointed out that quantitative analysis does not require any calibration work: cw-CRDS directly leads to absolute concentrations, provided that the target line strength is known (from HITRAN 2004 or GEISA databases for example [42, 43]). In the present work, the CO_2 absorption line at 6359.96 cm^{-1} was used with a line strength of 1.771×10^{-23} cm^{-1} molecule^{-1} cm^2 [39, 42] to derive the CO_2 concentration. As line strengths are given with an uncertainty of 5%, a similar uncertainty was reported on the corresponding concentration measurements.

CO_2 detection limit of our CRDS system has been calculated from the baseline noise level around 6360 cm^{-1}, by considering a signal height of three-times the noise amplitude. A detection limit of 6.6×10^{13} molecule cm^{-3} has been determined for CO_2 at 6359.96 cm^{-1}.

In order to evaluate the ability of our CRDS system to detect small changes in CO_2 concentrations, it was also necessary to estimate the repeatability of the measurements, as CO_2 was often present at the beginning of the experiments. The repeatability was calculated from a series of seven successive CO_2 measurements, leading to a standard deviation coefficient of 0.3%. Taking into account the uncertainties in the line strengths, the global uncertainty in CO_2 concentrations was estimated to be about 5%.

CH_3COOH *and* CH_3COOD. Determination of the concentrations of acetic acid and deuterated acetic acid has been performed using the thermal desorption – GC-FTIR analytical system. Calibration of the IR detector was carried out using standard solutions of these compounds in methanol. Response coefficients were obtained by plotting the area of the corresponding chromatographic peak versus the mass of the target compound at the detector. A good linearity has been obtained for both compounds.

Additional gas injections via the sample loop and the TCT injection system were carried out by sampling from the Teflon chamber filled with known amounts of acetic acid. The measured peak areas are consistent with the expected mass calculated from the concentrations of the compound in the simulation chamber. From the good agreement between the liquid and gas injections, it could be concluded that adsorption processes of acetic acid on the surface of the simulation chamber and along the Silcosteel sampling line were negligible. Un-

certainties in the quantification of acetic acids $CH_3C(O)OH$ and $CH_3C(O)OD$, estimated from repeated sampling from the simulation chamber and their analyses, were about 8% (2σ).

Detection limits DL were determined using a liquid standard with a concentration equal to five times the estimated DL. Seven replicate measurements of this standard were made, and the DL was calculated from the standard deviation σ of the replicate analyses as follow [44]:

$$DL = t\sigma$$

where t is the appropriate Student's value for a 99% confidence level ($t = 3.14$). The obtained detection limits for $CH_3C(O)OH$ and $CH_3C(O)OD$ are 213 μg and 288 μg at the detector, which correspond, respectively, to 1.0×10^{14} and 1.3×10^{14} molecule cm^{-3} in the environmental chamber.

3 Results and discussion

3.1 $CH_3C(O)OH + {}^{\bullet}OH$ *reaction*

Determination of the rate constant. The rate constant of the $^{\bullet}OH$-induced oxidation of acetic acid was first determined at 296 K using the relative rate method to validate our experimental set-up. The relative method [45] is based on the simultaneous measurement of the $^{\bullet}OH$ reaction rates of the target compound X (acetic acid in the present case) and a reference one R, the rate constant of the latter being well know and of the same order of magnitude of the investigated one.

$$X + OH \xrightarrow{k_X} \text{products},$$

$$R + OH \xrightarrow{k_R} \text{products}.$$

Assuming that the reactions of the target and the reference compounds with $^{\bullet}OH$ are the only routes of consumption of the studied compounds (photolysis processes and wall losses negligible, as check by controlled experiments), it can be shown that:

$$\ln \frac{[X]_0}{[X]_t} = \frac{k_X}{k_R} \ln \frac{[R]_0}{[R]_t},$$

where $[X]_0$ and $[R]_0$ and $[X]_t$ and $[R]_t$ are, respectively, the concentrations of the selected compound and the reference compound at time 0 and t, and k_X and k_R the rate constants of their reaction with $^{\bullet}OH$. A plot of $\ln([X]_0/[X]_t)$ versus $\ln([R]_0/[R]_t)$ yields a straight line with a slope of k_X/k_R.

The kinetic experiments were performed at (296 ± 2) K, using CH_3ONO as $^{\bullet}OH$ precursor and methanol as the reference compound. The recommended value of the rate constant for the reaction of CH_3OH with $^{\bullet}OH$ is $k_R = 9.0 \times 10^{-13}$ cm^3 $molecule^{-1}$ s^{-1} with an estimated uncertainty of about 15% (1σ) [19].

Because of the high initial acetic acid concentrations employed in our experiments, the formation of the acetic acid dimer in the reaction chamber should be taken into account. The dimerization of acetic acid is a fairly well characterized process, with the preferred value for the dimerization equilibrium constant K_{eq} given as [46]:

$$K_{eq} = \frac{P_D}{P_M^2} = 7.1 \times 10^{-9} \exp\left(\frac{7705}{T}\right),$$

where P_D and P_M are, respectively, the partial pressures (in atm) of the dimer and the monomer and T is the temperature in Kelvin. At 296 K, $K_{eq} = 1432.6$ atm^{-1} which is equivalent to 5.8×10^{-17} cm^3 $molecule^{-1}$ with an uncertainty of about 50%. It should be stressed that the analytical technique used in the present work to determine $CH_3C(O)OH$ concentrations was not able to differentiate the dimer from the monomer (the dimer is likely decomposed into the monomer in the thermodesorption step), so that the acetic acid measured concentrations $[CH_3C(O)OH]_{Total}$ were composed of the monomer and the dimer: $[CH_3C(O)OH]_{Total} = [\text{monomer}] + 2[\text{dimer}]$. Combining this relation and the above equation of K_{eq}, we derived the initial concentration of the acetic acid monomer $[\text{monomer}]_0$:

$$[\text{monomer}]_0 = \frac{-1 + \sqrt{1 + 8K_{eq}[CH_3C(O)OH]_{Total}}}{4K_{eq}}.$$

According to Singleton et al. [22], the reaction rate constant of $^{\bullet}OH$ radicals with the acetic acid dimer was approxi-

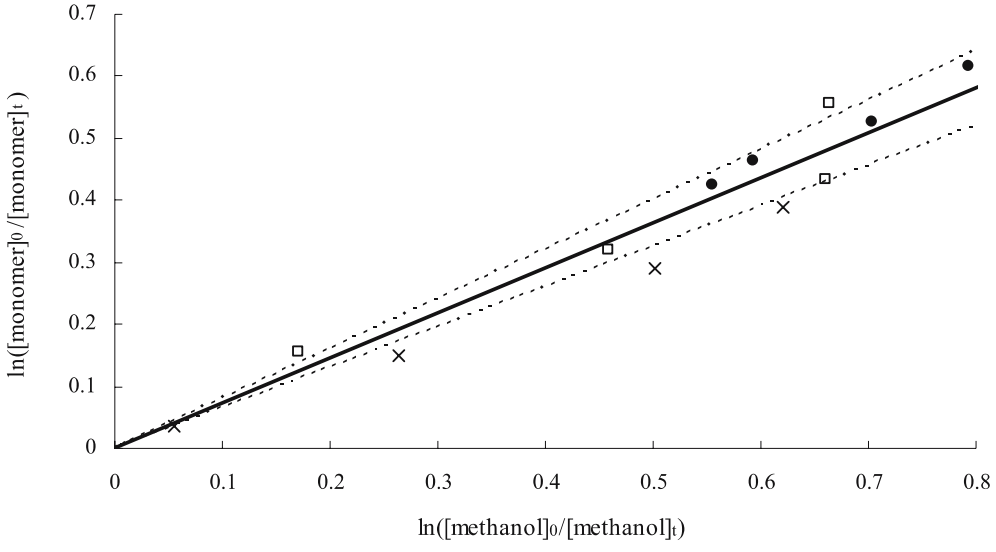

FIGURE 3 Relative rate plot for the reaction of OH with acetic acid at 296 ± 2 K using methanol as a reference compound. The *different symbols* represent each of the three experiments. The *solid line* represents the linear regression on the series of experiments and the *dashed lines* represent the confidence interval (2σ)

mately a hundred times less than that with the monomer ($k_{\mathrm{Dimer}} = 9.2 \times 10^{-15}\,\mathrm{cm^3\,molecule^{-1}\,s^{-1}}$) at ambient temperature. Thus, we considered that the observed consumption of $CH_3C(O)OH$ ($[CH_3C(O)OH]_{\mathrm{react}}$) corresponded only to the reaction of the monomer with $^{\bullet}OH$: $[CH_3C(O)OH]_{\mathrm{react}} = [\mathrm{monomer}]_{\mathrm{react}}$ and $[\mathrm{monomer}]_t = [\mathrm{monomer}]_0 - [CH_3C(O)OH]_{\mathrm{react}}$.

Figure 3 represents the results obtained for the three experiments carried out. The resulting rate constant ratio k_1/k_{R} is derived from the plot of $\ln([\mathrm{monomer}]_0/[\mathrm{monomer}]_t)$ versus $\ln([\mathrm{R}]_0/[\mathrm{R}]_t)$, where R represents the methanol. A linear regression for this group of data produced a value of $k_1/k_{\mathrm{R}} = 0.73 \pm 0.05$, giving a rate constant $k_1 = (6.5 \pm 0.5) \times 10^{-13}\,\mathrm{cm^3\,molecule^{-1}\,s^{-1}}$ (errors are twice the standard deviation of the linear regression). This value is in very good agreement with that of Butkovskaya et al. [20] of $6.6 \times 10^{-13}\,\mathrm{cm^3\,molecule^{-1}\,s^{-1}}$ and in the error limits of that recommended by Sander et al. [19] of $8.0 \times 10^{-13}\,\mathrm{cm^3\,molecule^{-1}\,s^{-1}}$. This result thus tends to prove that our experimental set-up is suitable for the investigation of the branching ratio of the reaction between acetic acid and hydroxyl radicals. The good agreement of our determination of k_1 with the literature data is also a clear indication of the correctness of the equilibrium constant value K_{eq} used to determine $[\mathrm{monomer}]_0$.

Determination of the branching ratio. The branching ratio R_1 of channel (1a) was defined as the ratio of the CO_2 formed to the $CH_3C(O)OH$ consumed in reaction (1):

$$R_1 = \frac{k_{1\mathrm{a}}}{k_{1\mathrm{a}} + k_{1\mathrm{b}}} = \frac{k_{1\mathrm{a}}}{k_1} = \frac{\mathrm{d}\,[CO_2]}{-\,\mathrm{d}\,[CH_3C(O)OH]} = \frac{[CO_2]_{\mathrm{formed}}}{[CH_3C(O)OH]_{\mathrm{react}}}\,.$$

Figure 4 represents an example of the time evolutions of $[CO_2]$ and $[CH_3C(O)OH]$. Before the formation of $^{\bullet}OH$ radicals by the photolysis of CH_3ONO, both concentrations are stable; at time 0, CH_3ONO is injected and simultaneously $CH_3C(O)OH$ starts to decrease and CO_2 to increase.

Determination of the branching ratio by the above method implies that the acetic acid consumption results only from reaction (1) and that CO_2 is only formed through channel (1a); this assumption is discussed further on. The results are presented on Fig. 5. By averaging over all experiments, we determined the branching fraction of reaction (1a) to be $R_1 = 78 \pm 13\,\%$. The quoted uncertainty corresponds to the standard deviation 1σ.

The obtained branching ratios are summarised in Tables 1 and 2 together with the two values available in the literature. Even though our value is slightly higher than those obtained by Butkovskaya et al. [20] and by De Smedt et al. [23], the agreement is still good within the experimental errors. Our result also confirms former findings [22, 47, 49] on the reactivity of acid dimers (formic and acetic) compared to acid monomers, that $^{\bullet}OH$ radicals interact mainly with the carboxylic hydrogen at ambient temperature.

The reason for the difference with the most recent investigations is not clear. First, it can be stressed that the experiments of Butkovskaya et al. [20] and De Smedt et al. [23] were carried out at low pressures (200 N_2 and 2 Torr He respectively), so that a small pressure effect on the branching ratio can be suspected. Another error source might arise from possible secondary reactions that can produce CO_2 in our reaction system. In particular, according to De Smedt et al. [23] (who referred to Peeters et al. [49] and to Olkhov et al. [50] (for reaction (5)), the pathway (1b) of the oxidation reaction could also form CO_2 in the presence of NO according to the following reaction scheme:

$$^{\bullet}CH_2C(O)OH + O_2 \rightarrow {}^{\bullet}OOCH_2C(O)OH\,, \quad (2)$$

$$^{\bullet}OOCH_2C(O)OH + NO \rightarrow {}^{\bullet}OCH_2C(O)OH + NO_2\,, \quad (3)$$

$$^{\bullet}OCH_2C(O)OH \rightarrow CH_2O + {}^{\bullet}C(O)OH\,, \quad (4)$$

$$^{\bullet}C(O)OH + O_2 \rightarrow CO_2 + HO_2^{\bullet}\,, \quad (5)$$

NO being present in our experiments due to the photolysis of CH_3ONO, the pathway (1b) could lead to the formation of CO_2.

However, some reasons drew us to suspect that the alkoxy radical $^{\bullet}OCH_2C(O)OH$ would rather react with O_2 than decompose. First, a heat of reaction for the decomposition reaction (4) of $\Delta H_{\mathrm{r}} = 51$–$83\,\mathrm{kJ\,mol^{-1}}$ can be calculated from the heat of formation of each compound involved in the reaction: $^{\bullet}OCH_2C(O)OH$: $\Delta H_{\mathrm{f}}^0 = -(376 \pm 8)\,\mathrm{kJ\,mol^{-1}}$ (personal communication with Tyndall, 2005),

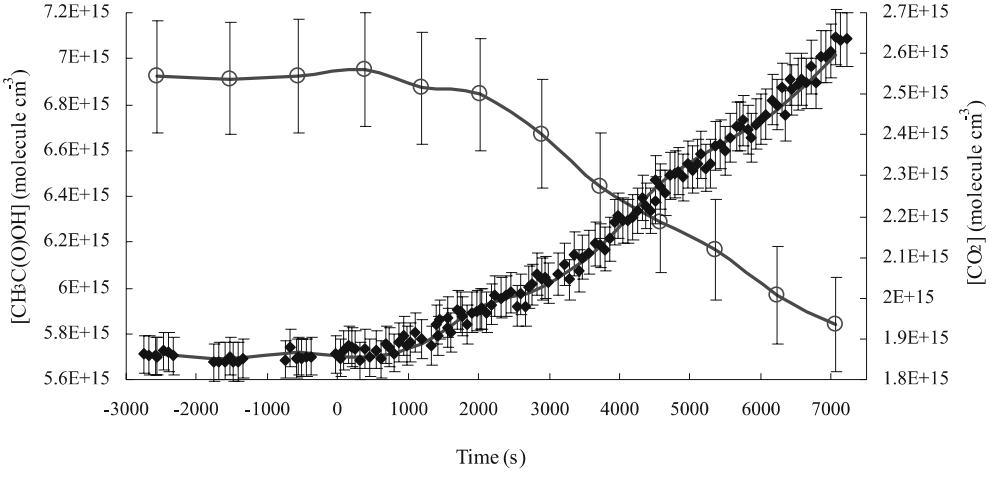

FIGURE 4 Plot of the acetic acid concentration (*open circle*) and CO_2 concentration (*black diamond*) versus reaction time. Time t_0 represents the beginning of the reaction by the photolysis of CH_3ONO and the consequent OH radical production

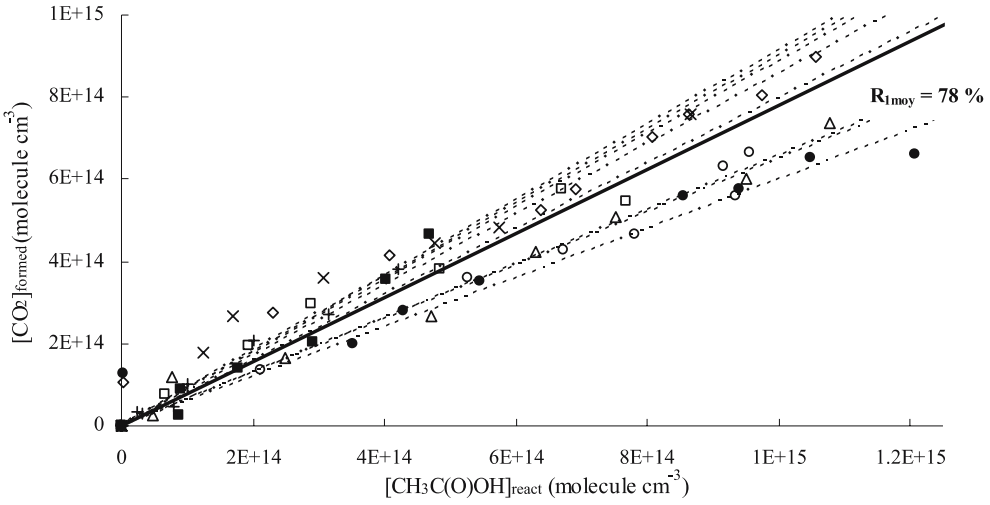

FIGURE 5 Plot of the amount of CO_2 formed against the amount of acetic acid reacted for a set of eight experiments. The *dashed lines* represent the linear regression on each experiment giving individual branching ratios and the *solid line* represents the average branching ratio

	$[CH_3C(O)OH]_0$ ($\times 10^{15}$ molecule cm^{-3})	$[CH_3ONO]_0$ ($\times 10^{14}$ molecule cm^{-3})	branching fraction of channel (1a) (%)
●	6.9	24.1	60
○	5.4	99.6	65
□	5.3	57.6	80
■	3.2	1.3	89
◇	6.9	73.4	86
△	6.9	1.4	66
+	6.2	12.2	90
×	5.2	1.2	91
		mean value	78
		standard deviation	13

TABLE 1 Initial experimental conditions for the set of experiments aiming at determining the branching ratio $R_1 = k_{1a}/k_1$ for the reaction between acetic acid and OH at (296 ± 2) K and atmospheric pressure

CH_2O: $\Delta H_f^0 = -117\,\mathrm{kJ\,mol^{-1}}$ [51] and $^\bullet C(O)OH$: $\Delta H_f^0 = -192 \pm 8\,\mathrm{kJ\,mol^{-1}}$ [52]. So, according to the thermochemistry the reaction (4) would only be possible at higher temperature than 296 K. Secondly, Tyndall et al. [53] also reported a study of the oxidation of methyl acetate, leading to the formation of $^\bullet OCH_2C(O)OCH_3$ radicals. They found that this radical does not decompose, but reacts with O_2 to form methyl glyoxylate. Another direct piece of evidence comes from Cavalli et al. [54], who photolysed methyl bromoacetate, leading to the formation of $^\bullet OCH_2C(O)OCH_3$ radicals: they also report a preferential reaction with O_2. Finally, it is interesting to note that we did not measure a 100% yield of CO_2. From the thermodynamic point of view and taking into account the studies quoted above on the $^\bullet OCH_2C(O)OCH_3$ alkoxy radical reactivity, we implied that the $^\bullet OCH_2C(O)OH$ radical formed in reaction (1b) will present a similar reactivity as the $^\bullet OCH_2C(O)OCH_3$ radical and would rather react with O_2:

$$^\bullet OCH_2C(O)OH + O_2 \rightarrow HC(O)C(O)OH + HO_2^\bullet, \qquad (6)$$

to form glyoxylic acid and $HO_2^\bullet$. Recently, Rosado-Reyes and Francisco (2006) [55] have performed ab-initio molecular calculations on the reaction of acetic acid with OH and have suggested that glyoxylic acid could be a major by-product of this reaction in atmospheric conditions. To test this hypothesis, we undertook complementary experiments aiming at detecting the glyoxylic acid HC(O)C(O)OH formed in reaction (6).

In these complementary experiments, $CH_3C(O)OH$ and $^\bullet OH$ have been left to react for 2 h, and after switching off the lamps, the reaction mixture was collected using a liquid trap: 50 mL of 10% CH_3OH in water was placed in a glass bubbler connected to a Teflon line. The reaction mixture was flown through the liquid at 500 mL min^{-1}. To minimise evaporation losses, the bubbler was placed in ice water. Analysis of the solution was achieved using ionic chromatography (DIONEX equipped with a AS11-HC column) coupled to conductime-

T (K)	P (Torr)	branching ratio (%)	reference	method
249–298	200	64 ± 17	Butkovkaya et al. (2004)	high-pressure turbulent flow reactor – $[CO_2]$ determination by chemical ionization mass spectrometer
290	2	64 ± 14	De Smedt et al. (2005)	multistage fast-flow reactor – $[CO_2]$ determination by molecular beam sampling mass spectrometer
296 ± 2	760	78 ± 13	this work	atmospheric smog chamber – $[CO_2]$ determination by cw-CRDS at 6359.96 cm^{-1}

TABLE 2 Branching ratio of the reaction between $CH_3C(O)OH$ and OH radicals

try detection. The elution solution consists of a concentration gradient of 1 mM of NaOH (2% MeOH) and 60 mM of NaOH (10% MeOH) flowing at 1.5 mL min^{-1}; the regeneration was obtained with a H_2SO_4 25 mM aqueous solution.

Glyoxylic acid was clearly identified and his presence in the liquid trap solution confirmed by the standard addition method. Possible interferences with other compounds of the mixture have been examined: the glyoxalate ion does not interfere with acetate, formate, nitrates, carbonates or nitrites ions. If a collection efficiency of 100% and good linearity of the method were supposed, a formation of glyoxylic acid corresponding to a yield of approximately 10% of the consumed acetic acid can be determined. This yield is the more consistent with the branching ratio of $R_1 = 78\%$ obtained previously since possible HC(O)C(O)OH wall losses (in the photoreactor or during the sampling) and reaction with $^{\bullet}$OH were not taken into account in this estimation. We conclude that our results strongly support the assumption that the $^{\bullet}OCH_2C(O)OH$ radical formed in reaction (1b) should react with O_2 and form glyoxylic acid.

3.2 $CH_3C(O)OD + {}^{\bullet}OH$ *reaction*

H-atom abstraction from the acid group being the major reaction path, a difference in the branching ratios of the reactions of $CH_3C(O)OH$ and $CH_3C(O)OD$ with $^{\bullet}$OH can be expected due to the kinetic isotope effect (KIE):

$$^{\bullet}OH + CH_3C(O)OD \rightarrow {}^{\bullet}CH_3 + CO_2 + HDO \quad (7a)$$

$$\rightarrow {}^{\bullet}CH_2C(O)OD + H_2O\,. \quad (7b)$$

The cw-CRDS instrument developed for the present study allowed us to measure CO_2 concentrations. The branching ratio R_7 of the pathway (7a) is thus determined by measuring the concentration ratio of the CO_2 formed ($[CO_2]_{formed}$) to the $CH_3C(O)OD$ reacted ($[CH_3C(O)OD]_{react}$):

$$R_7 = \frac{k_{7a}}{k_{7a}+k_{7b}} = \frac{k_{7a}}{k_7} = \frac{[CO_2]_{formed}}{[CH_3C(O)OD]_{react}} = \frac{[HDO]_{formed}}{[CH_3C(O)OD]_{react}}\,.$$

The initial conditions and corresponding obtained branching ratios are summarised in Table 3. The results are displayed on Fig. 6 by reporting $[CO_2]_{formed}$ versus $[CH_3C(O)OD]_{react}$. A branching ratio $R_7 = (36 \pm 7)\,\%$ was determined. To our knowledge, this study represents the first determination of the branching ratio of the CO_2-forming pathway in the $^{\bullet}OH + CH_3C(O)OD$ reaction. As expected for an H-atom abstraction reaction, the branching ratio R_7 for the reaction channel (7a) is smaller than that obtained for the non-deuterated acetic acid, and supports a strong primary kinetic isotope effect in the $^{\bullet}OH + CH_3C(O)OH$ reaction. Singleton et al. [22] investigated the rate constants of the reactions of $^{\bullet}$OH radicals with $CH_3C(O)OH$, $CD_3C(O)OH$ and $CD_3C(O)OD$ between 297 K and 444 K and observed roughly equal rates between $^{\bullet}OH + CH_3C(O)OH$ and $^{\bullet}OH + CD_3C(O)OH$. They quoted furthermore "the large kinetic isotope effect observed when the carboxylic but not the alkyl hydrogen is substituted by deuterium", for example in the case of $CD_3C(O)OH$ and $CD_3C(O)OD$. It should be emphasized that a large KIE was also observed for the formic acid when substituting a deuterium in the carboxylic group [48].

As mentioned in the experimental part, HDO could easily be detected at 6360.3 cm^{-1}, as well as around 6809 cm^{-1}.

		$[CH_3C(O)OD]_0$ ($\times 10^{15}$ molecule cm^{-3})	$[CH_3ONO]_0$ ($\times 10^{14}$ molecule cm^{-3})	branching fraction of channel (7a) (%)
CO_2 formation	○	5.4	57.6	28
	●	3.6	42.1	34
	△	1.2	69.1	45
	■	3.2	1.3	28
	×	5.2	1.2	42
				mean value 36
				standard deviation 7

TABLE 3 Experimental conditions and corresponding branching ratios for the oxidation of $CH_3C(O)OD$ by OH radicals at (296 ± 2) K and atmospheric pressure

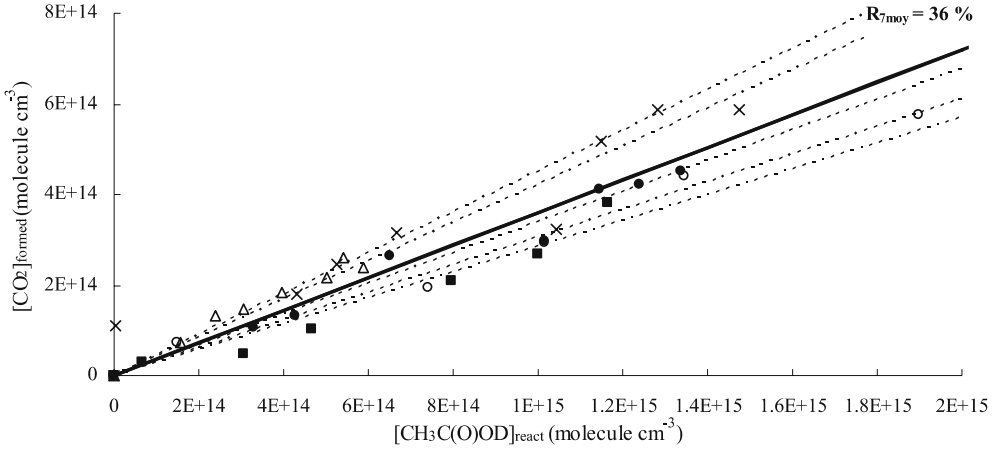

FIGURE 6 Plot of the amount of CO_2 formed against the amount of deuterated acetic acid reacted for a set of five experiments. The *dashed lines* represent the individual branching ratios and the *solid lines* the average branching ratios

The branching ratio R_7 of the pathway (7a) could thus also be determined by measuring the concentration ratio of the HDO formed ($[HDO]_{formed}$) to the $CH_3C(O)OD$ reacted. Additional experiments were then performed where both CO_2 and HDO were monitored. Consistent results were obtained when measuring HDO at 6809 cm^{-1} ($R_7 \approx 35\%$), but much smaller branching ratios were deducted from the measurements of HDO at 6360.3 cm^{-1} ($R_7 \approx 10\%$). This discrepancy could be attributed either to experimental complications or to uncertainties in the line strengths. Further experiments are in progress to resolve this disagreement.

4 Conclusion

A sensitive cw-CRDS apparatus in the near IR has been successfully built and coupled to a smog chamber to get new insights in the degradation mechanisms of atmospheric relevant organic compounds. The first study using this set-up has been devoted to the determination of the branching ratio of the $^{\bullet}OH$ oxidation reactions of $CH_3C(O)OH$ and $CH_3C(O)OD$ at atmospheric pressure and room temperature: branching fractions of $(78 \pm 13)\%$ and $(36 \pm 7)\%$ have been obtained for both acids, respectively. Glyoxylic acid has been detected for the first time as product of the pathway (1b).

Many interesting species, especially small isotopic molecules like $^{13}CO_2$, $H_2{}^{18}O$ and HDO can be observed in this chemical fingerprint spectral region, which can be very useful in the determination of reaction mechanisms. Possible future applications include in-situ investigation of reactions by following transient species such as $HO_2^{\bullet}$ or $CH_3C(O)O_2^{\bullet}$ radicals [56, 57]. Advantages of using CRDS include high sensitivity ($\approx 2 \times 10^{-8}$ cm^{-1} for our scheme but the highest sensitivity achieved using CRDS is 1×10^{-12} cm^{-1} $Hz^{-1/2}$) and rapidity of the measurement.

ACKNOWLEDGEMENTS The authors are deeply grateful to Mr. Thierry Leonardis and Dr. Olivier Briand from the Ecole des Mines de Douai and to Dr. Daniele Romanini from the Laboratoire de Spectrométrie Physique de Grenoble for their contributions to this work and their most helpful advise. Moreover, this work is jointly supported by the Nord-Pas de Calais region in the frame of the "Contrat de Plan Etat-Région, air quality axis", by the CNRS (Centre National de la Recherche Scientifique) in the frame of the "Programme National de Chimie Atmosphérique", by the CERLA (Centre d'Etudes et de Recherches Lasers et Applications – FR CNRS 2416), by the French Research Ministry and by the European funds for Regional Economic Development (FEDER). Sabine Crunaire gratefully acknowledges the financial support from the Ecole des Mines de Douai.

REFERENCES

1 H.B. Singh, M. Kanakidou, P.J. Crutzen, D.J. Jacob, Nature **378**, 50 (1995)
2 M. Narukawa, K. Kawamura, S.M. Li, J.W. Bottenheim, Atmos. Environ. **36**, 2491 (2002)
3 M. Ryhl-Svendsen, J. Glastrup, Atmos. Environ. **36**, 3909 (2002)
4 X. Yao, M. Fang, C.K. Chan, K.F. Ho, S.C. Lee, Atmos. Environ. **38**, 963 (2004)
5 A. Mellouki, G. Le Bras, H. Sidebottom, Chem. Rev. **103**, 5077 (2003)
6 G.C. Pratt, K. Palmer, C.Y. Wu, F. Oliaei, C. Hollerbach, M.J. Fenske, Environ. Health Persp. **108**, 815 (2000)
7 A. Chebbi, P. Carlier, Atmos. Environ. **30**, 4233 (1996)
8 P. Khare, N. Kumar, K.M. Kumari, S.S. Srivastava, Rev. Geophys. **37**, 227 (1999)
9 D. Grosjean, Atmos Environ. **26**, 3279 (1990)
10 J.N. Galloway, G.E. Liens, W.C. Keene, J.M. Miller, J. Geophys. Res. **87**, 8771 (1982)
11 X. Lee, D. Qin, G. Jiang, H. Zhou, Cold Reg. Sci. Technol. **34**, 127 (2002)
12 NTP 2003, National Toxicology Program, available at http://ntp.niehs.nih.gov:8080/index.html
13 K. Granby, C.S. Christensen, C. Lohse, Atmos. Environ. **31**, 1403 (1997)
14 K. Granby, A.H. Egeløv, T. Nielsen, C. Lohse, J. Atmos. Chem. **28**, 195 (1997)
15 G.S. Tyndall, R.A. Cox, C. Granier, R. Lescaux, G.K. Moortgat, M.J. Pilling, A.R. Ravishankara, T.J. Wallington, J. Geophys. **106**, 12 157 (2001)
16 R. Atkinson, J. Arey, Chem. Rev. **103**, 4605 (2003)
17 E.J. Feltham, M.J. Almond, G. Marston, V.P. Ly, K.S. Wiltshire, Spectrochim. Acta A **56**, 2605 (2000)
18 E.D. Baboukas, M. Kanakidou, N. Mihalopoulos, J. Geophys. Res. **105**, 14 459 (2000)
19 S.P. Sander, R.R. Friedl, D.M. Golden, M.J. Kurylo, R.E. Huie, V.L. Orkin, G.K. Moortgat, A.R. Ravishankara, C.E. Kolb, M.J. Molina, B.J. Finlayson-Pitts, *Chemical Kinetics and Photochemical Data for Use in Stratospheric Studies*, Evaluation No. 14 (JPL Publication 02-25, Pasadena, CA, 2003)
20 N.I. Butkovskaya, A. Kukui, N. Pouvesle, G. Le Bras, J. Phys. Chem. A **108**, 7021 (2004)
21 D.E. Heard, M.J. Pilling, Chem. Rev. **103**, 5163 (2003)
22 D.L. Singleton, G. Paraskevopoulos, R.S. Irwin, J. Am. Chem. Soc. **111**, 5248 (1989)
23 F. De Smedt, X.V. Bui, T.L. Nguyen, J. Peeters, L. Vereecken, J. Phys. Chem. A **109**, 2401 (2005)
24 A. O'Keefe, D.A.G. Deacon, Rev. Sci. Instrum. **59**, 2544 (1988)
25 D. Romanini, A.A. Kachanov, N. Sadeghi, F. Stoeckel, Chem. Phys. Lett. **264**, 316 (1997)
26 D. Romanini, A.A. Kachanov, F. Stoeckel, Chem. Phys. Lett. **270**, 538 (1997)
27 A. O'Keefe, Chem. Phys. Lett. **293**, 331 (1998)
28 J.B. Paul, L. Lapson, J.G. Anderson, Appl. Opt. **40**, 4904 (2001)
29 D.B. Atkinson, Analyst **128**, 117 (2003)
30 S.S. Brown, Chem. Rev. **103**, 5219 (2003)
31 B.L. Fawcett, A.M. Parkes, D.E. Shallcross, A.J. Orr-Ewing, Phys. Chem. Chem. Phys. **4**, 5960 (2002)
32 M.I. Mazurenka, B.L. Fawcett, J.M.F. Elks, D.E. Shallcross, A.J. Orr-Ewing, Chem. Phys. Lett. **367**, 1 (2003)
33 M.D. King, E.M. Dick, W.R. Simpson, Atmos. Environ. **34**, 685 (2000)
34 R. Claps, F.V. Englich, D.P. Leleux, D. Richter, F.K. Tittel, R.F. Curl, Appl. Opt. **40**, 4387 (2001)
35 H. Barry, L. Corner, G. Hancock, R. Peverall, G.A. D Richie, Phys. Chem. Chem. Phys. **4**, 445 (2002)
36 A.S.C. Cheung, T. Ma, H. Chen, Chem. Phys. Lett. **353**, 275 (2002)
37 A.R. Awatry, J.H. Miller, Appl. Phys. B **75**, 255 (2002)
38 Z. Majcherova, P. Macko, D. Romanini, V.I. Perevalov, S.A. Tashkun, J.L. Teffo, A. Campargue, J. Mol. Spectrosc. **230**, 1 (2005)
39 L.S. Rothman, D. Jacquemart, A. Barbe, D. Chris Benner, M. Birk, L.R. Brown, M.R. Carleer, C. Chackerian Jr., K. Chance, V. Dana, V.M. Devi, J.M. Flaud, R.R. Gamache, A. Goldman, J.M. Hartmann, K.W. Jucks, A.G. Maki, J.Y. Mandin, S.T. Massie, J. Orphal, A. Perrin, C.P. Rinsland, M.A.H. Smith, J. Tennyson, R.N. Tolchenov, R.A. Toth, J. Vander Auwera, P. Varanasi, G. Wagner, J. Quantum Spectrosc. Radiat. Transf. **96**, 139 (2005)
40 W.D. Taylor, T.D. Allston, M.J. Moscato, G.B. Fazekas, R. Kozlowski, G.A. Takacs, Int. J. Chem. Kinet. **12**, 231 (1980)
41 G. Berden, R. Peeters, G. Meijer, Int. Rev. Phys. Chem. **19**, 565 (2000)
42 HITRAN 2004, available at http://www.hitran.com
43 GEISA 2003, available at http://ara.lmd.polytechnique.fr
44 W.A. McClenny, J.D. Pleil, G.F. Evans, K.D. Oliver, M.W. Holdren, W.T. Winberry, J. Air Waste Manage. **41**, 1308 (1991)
45 R. Atkinson, W.P.L. Carter, A.M. Winer, J.N. Pitts, J. Air Waste Manage. **31**, 1090 (1981)
46 J. Chao, B.J. Zwolinski, J. Phys. Chem. Ref. Data **7**, 363 (1978)
47 G.S. Jolly, D.J. McKenney, D.L. Singleton, G. Paraskevopoulos, A.R. Bossard, J. Phys. Chem. **90**, 6557 (1986)
48 D.L. Singleton, G. Paraskevopoulos, R.S. Irwin, G.S. Jolly, D.J. McKenney, J. Am. Chem. Soc. **110**, 7786 (1988)
49 J. Peeters, G. Fantechi, L. Vereecken, J. Atmos. Chem. **48**, 59 (2004)
50 R.V. Olkhov, Q. Li, M.C. Osborne, I.W.M. Smith, Phys. Chem. Chem. Phys. **3**, 4522 (2001)
51 M.W. Chase Jr., J. Phys. Chem. Ref. Data **9**, 1 (1998)
52 Y. He, B.J. Orr, Chem. Phys. Lett. **319**, 131 (2000)

53 G.S. Tyndall, A.S. Pimentel, T.J. Orlando, J. Phys. Chem. A **108**, 6850 (2004)
54 F. Cavalli, I. Barnes, K.H. Becker, T.J. Wallington, J. Phys. Chem. A **104**, 11 310 (2000)
55 M. Rosado-Reyes, J.S. Francisco, J. Phys. Chem. A **110**, 4419 (2006)
56 D.B. Atkinson, J.L. Spillman, J. Phys. Chem. A **106**, 8891 (2002)
57 S.J. Zalyubovsky, B.G. Glover, T.A. Miller, J. Phys. Chem. A **107**, 7704 (2003)